WPMST1-CPR(17) 17289

A Kallenbach et al.

Parameter dependences of the separatrix density in nitrogen seeded ASDEX Upgrade H-mode discharges

Preprint of Paper to be submitted for publication in Proceeding of 44th European Physical Society Conference on Plasma Physics (EPS)

This work has been carried out within the framework of the EUROfusion Consortium and has received funding from the Euratom research and training programme 2014-2018 under grant agreement No 633053. The views and opinions expressed herein do not necessarily reflect those of the European Commission.

Parameter dependences of the separatrix density in nitrogen seeded ASDEX Upgrade H-mode discharges

A. Kallenbach[1], **H.J. Sun**[1], **D. Carralero**[1], **T. Eich**[1], **J. Hobirk**[1], **A. Scarabosio**[1], **M. Siccinio**[1], **ASDEX Upgrade team**[2], **EUROfusion MST1 team**[3]

[1]Max Planck Institute for Plasma Physics, D-85748 Garching, Germany,
[2]A. Kallenbach et al., Nucl. Fusion **57** (2017) 102015
[3]H. Meyer et al., Nucl. Fusion **57** (2017) 102014

Abstract. The upstream separatrix electron density is an important interface parameter for core performance and divertor power exhaust. It has been measured in ASDEX Upgrade H-mode discharges by means of Thomson scattering using a self-consistent estimate of the upstream electron temperature under the assumption of Spitzer-Härm electron conduction. Its dependence on various plasma parameters has been tested for different plasma conditions in H-mode. The leading parameter determining $n_{e,sep}$ was found to be the neutral divertor pressure, which can be considered as engineering parameter since it is determined mainly by the gas puff rate and the pumping speed. The experimentally found relationship $n_{e,sep} \propto p_0^{0.31}$ could be approximately reconciled by 2-point modelling. Fitting of the measured separatrix density by 1D modelling, which yields an estimate for momentum losses and radiative power losses, suggests a broadening of the heat flux width in the divertor which increases with neutral pressure.

1. Introduction

A very important interface parameter between core plasma performance and divertor power exhaust is the electron density at the outer midplane separatrix, $n_{e,sep}$. In a most simple and qualitative picture, a low separatrix density is beneficial for the plasma energy confinement [1] [2], while a high density enables and supports the achievement of divertor detachment [3] [4] [5] [6]. An important tokamak operational limit, the H-mode density limit, is also connected to an upper limit of the separatrix density [7] [8]. The power exhaust is also closely coupled to the divertor neutral pressure or neutral fluxes: The power flux in the outer divertor at the detachment threshold was found to scale about linearly with the weighted pressures of deuterium and nitrogen [9] [10]. Neutral divertor fluxes can be regarded as superior parameters for the description of power dissipation since the divertor losses are closer linked to fluxes than to densities (relevance of the radiative potential [11] [12] instead of loss function L_z). In addition, impurity fluxes are better known in the divertor in comparison to impurity concentrations. Therefore, it is of great interest to establish the relation between divertor neutral pressure and the upstream separatrix density in order to achieve a better integration of energy confinement and exhaust optimization.

Direct measurements of the (upstream) separatrix density are not easily available. The major experimental problem stems from the correct assignment of the separatrix position from equilibrium reconstruction, which suffers uncertainties comparable to the radial density decay length. To overcome this problem, Thomson scattering is used which measures T_e and n_e at the same location, while the separatrix position is assigned via the power flux P_{sep} and an assumption for the width of the power carrying layer [13] [14] [15] [16].

The lack of a large experimental data base of the separatrix density is the reason for a lack of scalings of this quantity with engineering parameters like machine radius R or plasma current I_p. Based on experience on present day tokamaks, a constant fraction of separatrix density and Greenwald density, $n_{e,sep}/n_{GW}$ is often assumed [5]. Due to the large I_p ratio between current experiments and, e.g., ITER, the parameter dependence of $n_{e,sep}$ on I_p is of particular importance. Regarding power exhaust, in addition to the separatrix density, the power width λ_q and the divertor broadening S are important [10]. λ_q was found to scale roughly with the inverse poloidal magnetic field, $1/B_p$, and thus $\lambda_q \propto 1/I_p$ for constant geometry [17].

In this paper, an experimental data base is presented of nitrogen seeded AUG H-mode discharges with sufficiently constant seeding level for the achievement of nearly steady state conditions and n_e, T_e measurements by the edge Thomson scattering system [18]. The separatrix electron density is here evaluated at the location of $T_{e,sep}$ as inferred from power balance, taking the power width λ_q as 2/7 of the measured λ_{Te} under the assumption of parallel Spitzer-Härm thermal conduction [16]. The experimental data base is described in section 2. Emphasis is placed on the divertor neutral pressure, which can be regarded as an engineering parameter in devices with a closed divertor and active

pumping. Simple 2-point considerations are presented in section 3 for the relation of the upstream separatrix density and the divertor neutral flux. The spatial neutral flux distribution, which is effected by the high field side high density region (HFSHD) [19] is discussed in section 4. Finally, in section 5 an attempt is presented to derive by means of 1D modelling the divertor heat flux broadening from the measured upstream $n_{e,sep}$. Some conclusions are drawn in section 6.

2. Experimental data base

When inspecting outer divertor detachment behaviour, the most important input is the parallel heat flux arriving at the divertor entrance. Its radial decay length, λ_q, has been very well characterized in the past using IR thermography, starting from the divertor surface side, and robust scalings for fully attached H-mode conditions are available [17] [20]. The target heat flux can for sufficiently collisional conditions be related to the power flux over the separatrix, P_{sep}, assuming Spitzer-Härm parallel electron heat conduction [18]. For conditions of non-negligible divertor radiation or momentum losses, IR measurements can no longer be directly related to the heat flux at the divertor entrance. These are the conditions of interest in this study. A data base was set up

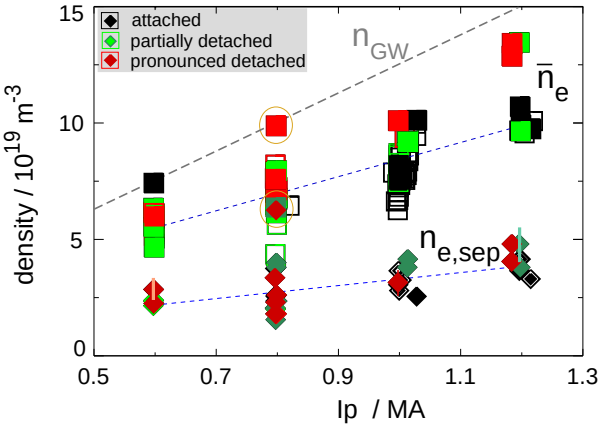

Figure 1. *Line-averaged (squares) and separatrix (darker color, diamonds) densities versus plasma current in the data base. Full symbols denote data base entries with $n_{e,sep}$ data. Blue dotted lines are (offset) linear fits to guide the eye. Golden circles denote line-averaged and separatrix density very close to the H-L density limit, # 34613 t=3.8-3.95 s.*

of ASDEX Upgrade H-mode discharges from 2014-2017 (divertor III) with different deuterium gas puff and nitrogen seeding levels, plasma currents and separatrix crossing power, P_{sep}. Time intervals of typically 0.5 s duration are considered, where D and N gas puff levels are sufficiently stationary and in balance with pumping. Of special interest here are discharges with good quality of the edge Thomson scattering data for the determination of electron temperature and density fall-off widths, λ_{Te} and λ_n [18]. Thomson scattering data are evaluated using a simple 2-point scaling. The power to the outer divertor is taken as the difference of heating power and total radiated power,

assuming that all the power flowing towards the inner divertor is radiated. The power width is taken as 2/7 of the measured λ_{Te} according to Spitzer-Härm conduction [16]. Figure 1 shows the line-averaged and the separatrix densities of the data base versus the plasma current. With significant variations, both densities rise roughly proportional to the plasma current. The highest line-averaged densities approaching the Greenwald density are obtained under pronounced detachment conditions [9]. The uncertainty of $n_{e,sep}$ is typically +15, -20 %, where the asymmetry results from the assumption that the fraction of P_{sep} flowing to the outer divertor is delivered to the electron channel, thus $T_{e,sep}$ being at its upper limit and hence $n_{e,sep}$ evaluated at a high value, accordingly.

Figure 2 compares the Spitzer-Härm power decay length with the prediction of the Eich scaling [17] for nitrogen seeded discharges with different gas puff levels, heating powers, plasma current etc. Due to the partly very high ELM frequencies and small ELM amplitudes, no effort was taken to cut out ELM effected time points from the Thomson scattering data, as done in [18]. Good agreement is observed, albeit a trend towards higher values derived from Thomson scattering compared to the Eich prediction for higher plasma currents is visible.

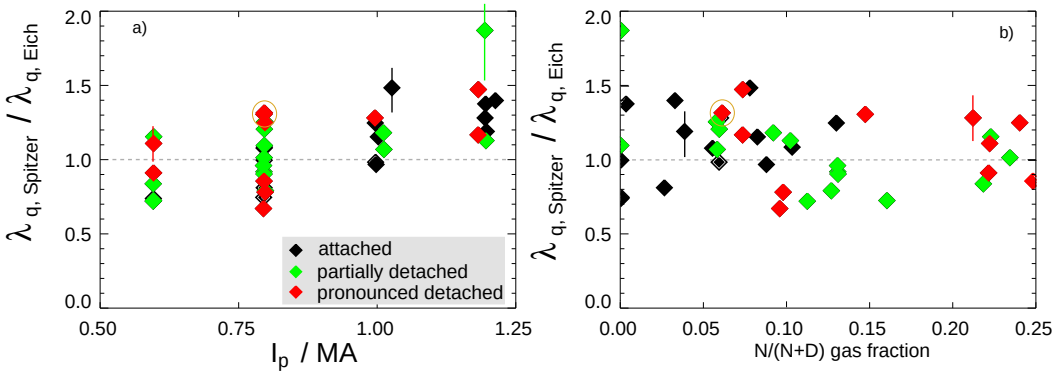

Figure 2. *a) Comparison of power decay lengths λ_q derived from Thomson scattering assuming Spitzer-Härm parallel electron heat conduction with the prediction of the Eich scaling for discharges with partially strong N and D puffing and different degrees of detachment. Absolute values of the reference $\lambda_{q,Eich}$ vary from about 3.3 mm (0.6 MA) to 1.7 mm (1.2 MA) measured in radial direction in the outer midplane. Error bars denote typical statistical errors, a possible contribution of ELMs to the derived width is not included. b) Deviation of $\lambda_{q,Spitzer}$ from the Eich scaling vs. nitrogen atomic fraction in the divertor gas. No trend with the gas fraction, which approximates the N concentration in the divertor plasma [10], is observed.*

Different parameter variations have been tested to identify a physics parameter responsible for the moderate deviation from the Eich scaling at high I_p. As shown in figure 2b, $\lambda_{q,Spitzer}$ / $\lambda_{q,Eich}$ shows no significant trend with nitrogen content or degree of detachment (color coded). We conclude that the most probable cause of the deviation is the influence of ELMs on the measured temperature decay length. Such an influence is expected to be larger at higher I_p, where the inter-ELM decay length is shorter. It should be noted that a corresponding deviation was not observed in the analysis shown in [18],

where a more regular ELM behaviour allowed to leave out ELM-affected time points. The discharges shown here have acceptable or good H-mode confinement with $H_{98} \geq 0.8$ thanks to N seeding and high heating power. A broadening of $\lambda_{q,Spitzer}$ presented for a few discharges in [18] is connected to strong energy confinement degradation during detachment, with $H_{98} \approx 0.5$. Obviously, the processes responsible for the pedestal degradation also increase λ_q.

Various regression tests of the upstream separatrix density determined from Thomson scattering versus experimental parameters revealed the neutral divertor pressure, p_0, measured by a baratron connected by a 0.5 m pipe below the high field side divertor, as leading parameter, see figure 3. p_0 can be regarded as engineering parameter since it is largely set by the gas puff level and the applied pumping speed. A baratron is used here since it not disturbed by the presence of nitrogen in contrast to ionization gauges. There is an experimental trend of higher neutral pressure at higher currents, but this is produced by operational constraints (like, e.g., the necessity to puff gas to avoid tungsten accumulation at higher plasma currents). The scaling obtained is $n_{e,sep} = 2.65\ p_0^{0.31}$ (10^{19} m^{-3}, Pa). In an earlier study, the averaged SOL density from Li beam measurements had been compared to the neutral flux density below the divertor roof baffle [1]. A relation $n_{e,SOL} \propto \Gamma_0^{0.55} q_{95}^{0.68}$ had been observed, not far from the present result except the q_{95} dependence. A possible explanation for this deviation may be the fact that the separatrix density depends strongly on the short decay length λ_n, which shrinks with I_p, while $n_{e,SOL}$ is also effected by profile wings or shoulders.

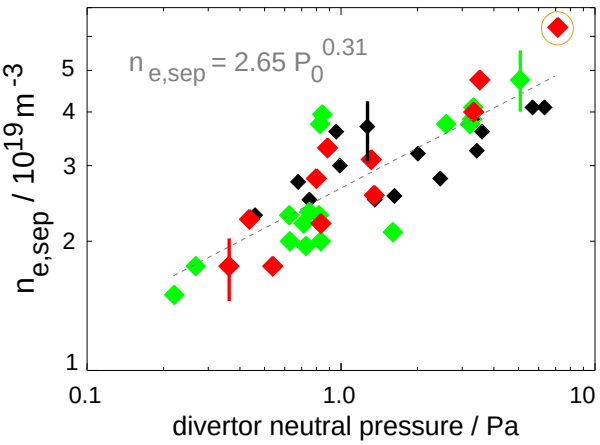

Figure 3. *Dependence of the upstream separatrix density on divertor pressure, measured by a baratron below the roof baffle region.*

In a simple picture of tokamak gas balance, in equilibrium the divertor neutral pressure is proportional to the gas puff rate, with the effective pumping speed as constant of proportionality. Figure 4 compares the measured neutral pressure with the gas puff rate, the expectation for a pumping speed between 20 and 30 m^3/s is indicated by a grey bar. In reality, the simple relation is modified by uptake or release of gas by the walls [21] and a weak pressure dependence of the pumping speed. In addition, the pressure

measured by the baratron is effected by neutrals produced in the vicinity of the high field side high density region, see section 4.

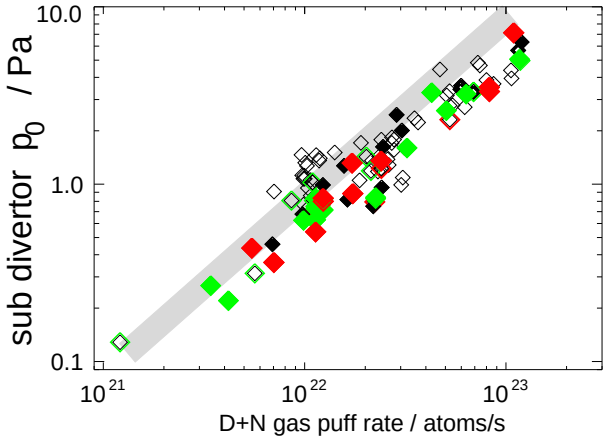

Figure 4. *Dependence of the divertor pressure measured by a baratron below the roof baffle region and the sum of N an D gas puff rates. The grey line shows the expected pressure for a constant effective pumping speed of 20-30 m^3/s, which is the expected range with full cryopump active. For a few data points with 1/3 cryo pump active, the gas puff rates have been divided by the estimated effective pumping speed fraction, 0.5, for the shot with cryo off (marked by circle) by 0.3, respectively. Measurement uncertainties of pressure and gas fluxes are of the order of the symbol sizes. NBI fuelling has been neglected.*

Figure 5 shows the separatrix density normalized by its neutral pressure dependence versus the plasma current, the non-radiated power crossing the separatrix and the strike point location at the target. The very weak dependence of the normalized separatrix density on I_p and P_{sep} suggests that the rise of $n_{e,sep}$ with I_p shown in figure 1 is caused by the increased gas puff / recycling level. There is also no significant dependence on the strike point location.

3. Expectations from simple analytical considerations

In the following, the observed experimental trend between the upstream separatrix density n_{mid} and the neutral divertor pressure, p_0 is derived using simple 2-point model considerations [22], assuming dominant electron conduction and T_e=T_i [eV]. The present treatment differs from recent work [15] regarding the use of 'enginering parameters', namely the neutral flux rather than the divertor T_e.
The plasma parameters in the divertor and midplane are closely coupled by pressure balance and heat conduction. Momentum losses and divertor radiation are considered via simple multiplier / loss factors f_{mom} and f_{rad} between outer midplane and sheath in front of the target:

$$f_{mom} = 2n_{div}T_{div}/(n_{mid}T_{mid}), \quad f_{rad} = 1 \; - \; bq_{\|,div}/q_{\|,mid} \tag{1}$$

A Mach=1 flow towards the target at the sheath is assumed, resulting in a reduction of the static pressure by a factor 2. We have also introduced a divertor heat flux broadening

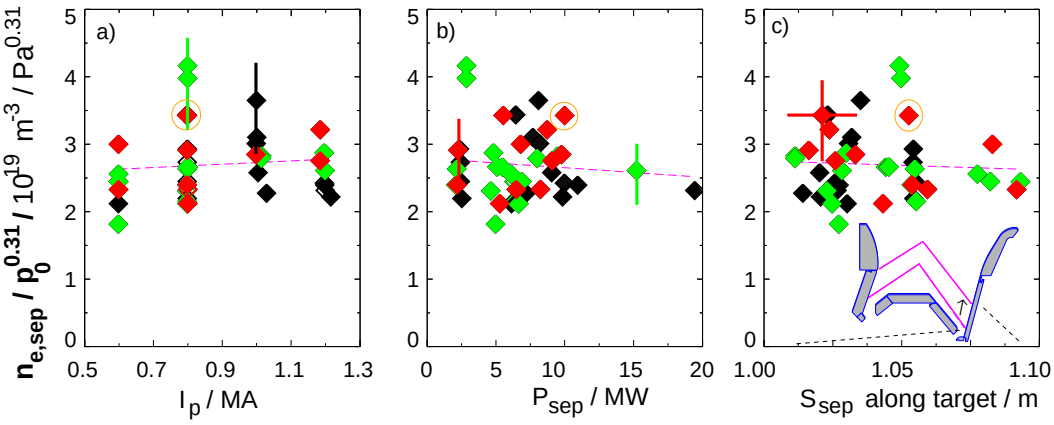

Figure 5. *Separatrix density from Thomson scattering normalized by its neutral pressure dependence versus a) plasma current, b) separatrix power and c) position of the outer strike point along the target. The dashed lines are offset-linear fits, showing the weak dependence of the normalized n_{sep} on I_p and P_{sep}.*

factor $b = \lambda_{int}/\lambda_q \approx 1 + 1.64S/\lambda_q$ with the exponential decay λ_q and the Gaussian broadening S [17] [23]. The midplane temperature is approximated assuming Spitzer electron conductivity along the connection length L and the divertor heat flux is given by the sheath boundary condition:

$$eT_{mid} = e(\frac{7}{2\kappa})^{2/7} \ (Lq_{\parallel,mid})^{2/7} \tag{2}$$

$$q_{\parallel,div} = \gamma(2/m_D)^{0.5} \ n_{div}(eT_{div})^{3/2}, \ \kappa = 2380\frac{W}{m \ eV^{7/2}} \tag{3}$$

γ is the sheath energy transmission factor which is typically between 7 and 8, but can be as low as 4.6 for a tungsten surface when about 50 % of the ion energy is reflected [24]. We want to establish a connection to the neutral pressure. For this we make the assumption that the neutral flux density, Γ_0 measured in the sub-divertor equals the ion flux density perpendicular to the target, as will be discussed below.

$$\Gamma_0 = \ sin(\alpha) \ q_{\parallel,div}/(\gamma \ eT_{div}) = \ (1 - f_{rad}) \ sin(\alpha) \ q_{\parallel,mid} \ /(b \ \gamma \ eT_{div}) \tag{4}$$

α is the impact angle of the field line at the outer target, a typical value is 2.5^o. The radiative losses, which include in this simple treatment the power loss due to charge exchange and ionisation, are described by f_{rad}. Finally, by combination of eqns 1-3, we obtain for the upstream density

$$n_{mid} = \frac{2}{f_{mom}} (1-f_{rad})^{1/2} \frac{1}{e}(\frac{2\kappa}{7L})^{2/7} (m_D/2)^{0.5} (b\,\gamma \sin(\alpha))^{-1/2} q_{\parallel,mid}^{3/14} \Gamma_0^{1/2} \tag{5}$$

Eq. 5 quite well reconciles the experimental finding for n_{mid} shown in figure 3 that the separatrix density depends mainly on the neutral flux. There is only a weak I_p dependence expected via $q_{\parallel,mid} \propto P_{sep}/\lambda_q$, $\lambda_q \propto 1/B_p \propto 1/I_p$. The f_{mom} and f_{rad} dependencies partly cancel, since an increase in f_{rad} usually causes a reduction in f_{mom} [3]. The difference in the exponent for the neutral flux dependence between model and

experiments (0.5 vs. 0.31) requires further consideration. For comparison with the experimental pressure measurement, first the neutral flux density Γ_0 (assumed equal to the perpendicular ion flux to the target) is linearly converted into a neutral pressure measured at the baratron location (molecules at room temperature in a remote pipe below the inner divertor region) by the relation $\Gamma_0 = p_0\ 1.5\ 10^{23}$ atoms $m^{-2}\ s^{-1}$ / Pa. For a number of discharges with strike point sweeps allowing to measure profiles along the target, ion flux densities can be directly compared to the neutral pressure measurement. Figure 6 compares the peak ion flux density measured by Langmuir probes in the outer divertor (median filtered to reduce the impact of ELMs) with the neutral pressure measured by the baratron. Quite close absolute agreement is found for attached conditions when the conversion factor is applied, but the neutral pressure rises slightly faster than the ion flux density $p_{0,max} \approx j_{sat,max}^{1.25}$. So far we have considered

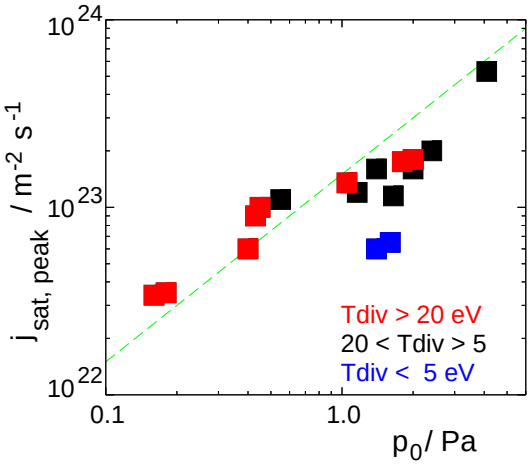

Figure 6. *Peak ion flux density from Langmuir probes versus the neutral pressure measured in a vertical port below the inner roof baffle. The green line shows the predicted ion flux density under the assumption of equal flux densities at the target and the baratron location (300 K molecular flux). Small data set due to the requirement of a strike point sweep for the identification of* $j_{sat,max}$.

neutral flux densities, since these are directly measured quantities. For the present divertor conditions, we expect a balance of *total* recombining ion fluxes and ionising neutral fluxes, see below in section 5, fig. 10b. A quantitative assessment of these fluxes would require a 2D modelling with, e.g., the SOLPS code. The present data set has been modelled with a simpler 1D code to shed light on the dependencies of fluxes and pressure, as will be shown below in section 5.

4. Effects of seeding on neutral gas and fueling

The effect of nitrogen seeding on the energy confinement has been at least partly attributed to a reduction of the separatrix density, which results in a favorable alignment of edge pressure and current profiles [2]. To shed further light on the relation of N

seeding, neutral fluxes and $n_{e,sep}$, a well diagnosed discharge pair is investigated in more detail. Figure 7 compares traces of two discharges with and without nitrogen seeding using Tdiv feedback control [25]. Langmuir probe data along the outer target

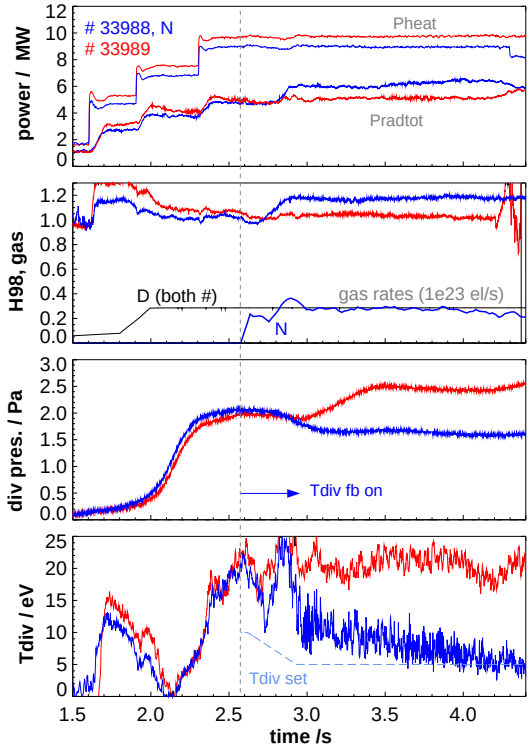

Figure 7. *Comparisons of 2 discharges with and without N seeding. Measured upstream separatrix densities from TS are 2.1 (with N) and 2.9 10^{19} m^{-3} (w/o N). I_p= 0.6 MA.*

for both discharges are shown in figure 8. The seeding of nitrogen has an influence on the spatial distribution of neutral fluxes, as shown in figure 9. The reduction of the neutral flux density below the inner heat shield is attributed to a reduction of the high field side high density region [26] [19] [27]. This reduction also effects the baratron neutral pressure measurement below the high field side divertor region. In contrast, the ionisation gauge signals below the roof baffle and in the pump chamber rise due to contribution of nitrogen. Since the D puff is kept constant, particle balance suggests an about constant contribution of D to the gauge signals with and without N puffing. During N seeding, the separatrix density decreases despite a constant D puff. This is attributed to the reduced fueling effect of the high field side high density [27]. The fact that this contribution is caught by using the neutral pressure at the location of the baratron in the scaling obtained may be coincidence. Currently, it is not clear to which extent the HFSHD contributes to $n_{e,sep}$ via neutral and via diffusive ion fueling.

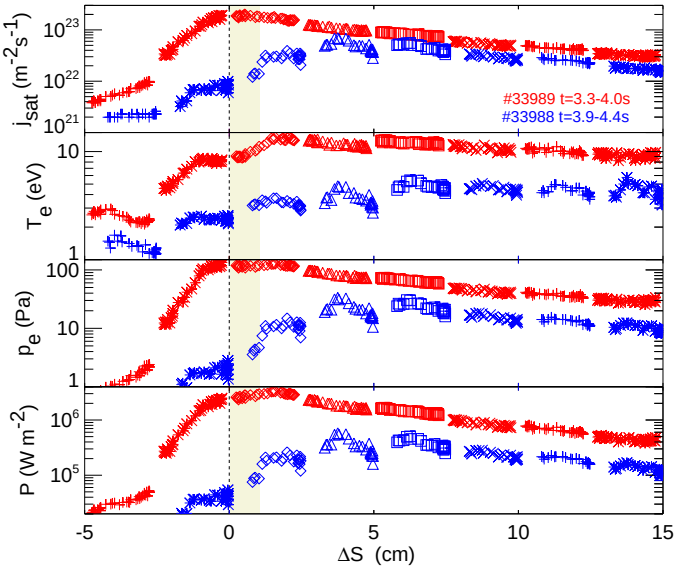

Figure 8. *Langmuir triple probe data for the discharge pair introduced in figure 7. Data are median filtered over 20 ms to eliminate small excursions due to the small ELMs. The shaded bar indicates the first power e-folding length* λ_q.

5. Divertor heat flux broadening

Equation 5 predicts a dependence of the upstream separatrix density on the divertor heat flux broadening factor b. Since this parameter is not well known and understood, we derive its estimate from the measured separatrix density using a simple 1D SOL flux tube model. Input to the 1D model [10] are the power to the outer divertor within the first power width, estimated as $P_{sep}/2.3$, λ_q from Thomson scattering assuming Spitzer-Härm parallel conduction and the divertor nitrogen concentration estimated by the valve flux ratio. A closed divertor geometry is assumed, i.e. all neutrals produced in the outer divertor are ionised there. All datapoints from figure 3 are used. The 1D model calculates among others the coefficients f_{rad} and f_{mom} introduced in section 3. The divertor broadening factor b is applied up to a target distance of 5 m along the flux bundle, which corresponds to the divertor region below the X-point. The N concentration in the model has been increased by 0.01 to take into account other low-Z intrinsic impurities. The only free parameter left in the 1D model is the divertor broadening b or total power width λ_{int}, which is adapted to match the measured upstream $n_{e,sep}$. Figure 10a shows the broadening b written as the ratio of λ_{int} and the prediction of λ_q at the divertor entrance from the Eich scaling. Increasing broadening is observed with increasing neutral pressure. This broadening should not be confused with the S factor in the Eich fit function [17], since for the present conditions power and momentum losses are present. Without losses, the simple approximate relationship $\lambda_{int} = 1.64S + \lambda_q$ holds [23]. A broadening is obtained which increases with divertor neutral pressure. The uncertainties indicated in figure 10 are not easy to assess and thus have to be regarded as estimates. The effect of the input upstream λ_q has been tested

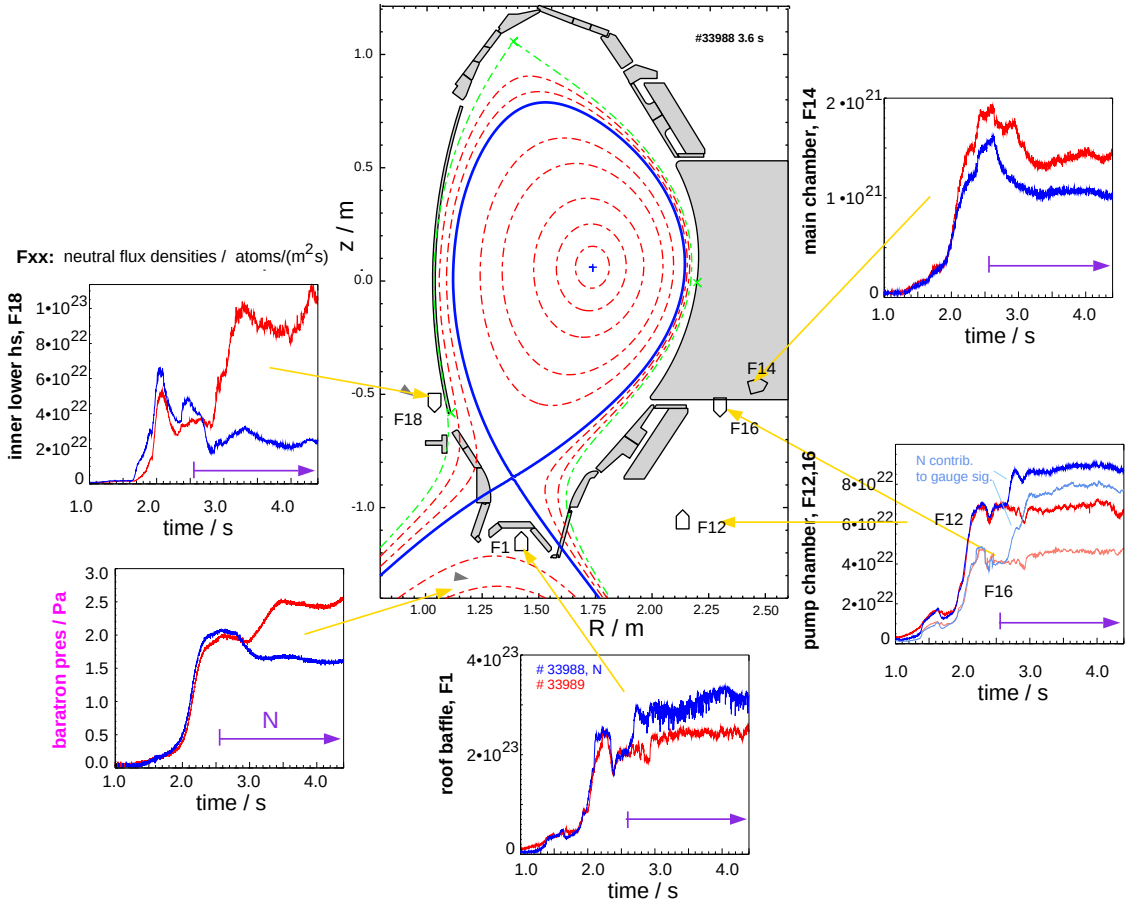

Figure 9. *Neutral fluxes for the discharge pair introduced in figure 7. The ionisation gauges also measure nitrogen (sensitivity for N pressure about a factor 2.4 higher compared to D), which explains the rise in the divertor gauge signals after start of the N puff.*

by repeating the fit with the predicted λ_q from the Eich scaling instead of 2/7 λ_{Te} from Thomson scattering (deviation shown in figure 2a). The obtained variation of λ_{int} are $\pm$ 10 %. The most uncertain input quantity is the divertor nitrogen concentration, as estimated from the relative gas valve fluxes. Changing this input parameter by $\pm$ 30 % under highly radiative conditions, a variation of λ_{int} by $\pm$ 15 % is obtained. The major part of the uncertainty of the determination of the broadening b using 1D model calculations is assumed to result from the neutral model, and expected to increase with deepening of the detachment.

Figure 10b shows the neutral flux density and the total neutral flux at the target plate for the first 1/e power e-folding width for the model data base compared to the measured neutral pressure. The flux density Γ_0 corresponds in absolute scale roughly to the pressure (conversion 1.5 10^{23} at/(m^{2}s) per Pascal), but exhibits a weaker slope. The deviation from a linear relationship corresponds to the $\Gamma_0^{0.5}$ dependence of $n_{e,sep}$ in the model compared to $p_0^{0.31}$ in the experiment. A better concordance is obtained if the total neutral flux is correlated with the pressure measurement, but 2D modelling would

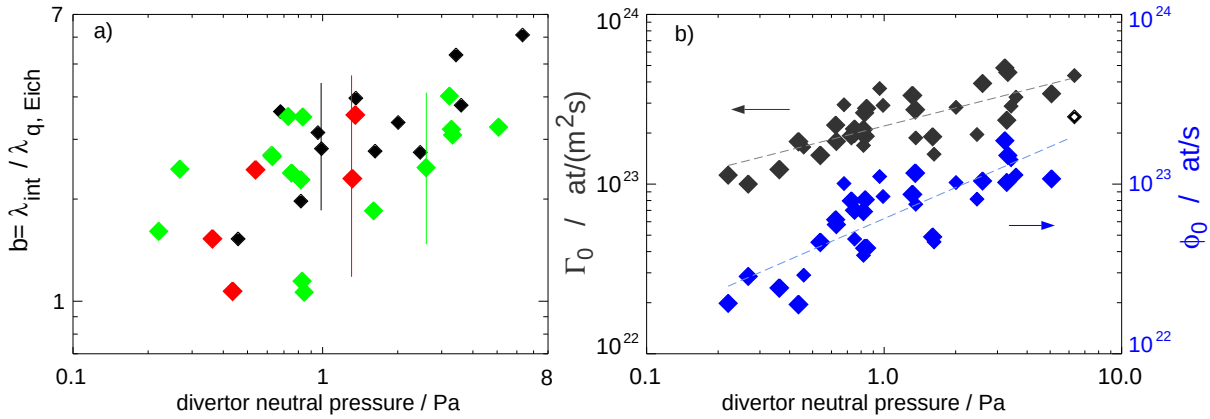

Figure 10. *a) Divertor broadening* $b = \lambda_{int}/\lambda_{q,Eich}$ *and b) neutral fluxes and flux densities from 1D modelling versus the measured divertor neutral pressure.* λ_{int} *was obtained from 1D modelling fitting the measured upstream* $n_{e,sep}$*. Error bars are estimates only, uncertainties increase with detachment and radiative fraction. The total fluxes were obtained by multiplication of the flux densities in the flux bundle with the target wetted area of this bundle, which increaes with b.*

be required to disentangle the neutral transport effects on an absolute scale. One has to keep in mind that effects of the HFSHD on the pressure measurement are also not included in the 1D model. Nevertheless, the introduction of the divertor broadening b= λ_{int}/λ_q is essential for the achievement of approximate consistency of 1D modelling with the experimental data.

The physics origin of the obtained broadening cannot be judged from the simple 1D model analysis. It could be caused by diffusive transport, radial transport related to blobs [28] [29], neutral/molecular effects or radiative losses which are not correctly captured by the 1D model. Nevertheless, the increase of b with neutral pressure suggests that the use of just λ_q for divertor heat flux estimates is too pessimistic. Substantial divertor heat flux broadening not only increases the target power width, but also leads to enhanced radiative losses due to an increase of the radiating volume [10].

6. Conclusions

Measurements of the upstream separatrix density for N seeded and unseeded H-modes reveal a strong correlation with the divertor neutral pressure, $n_{e,sep} \propto p_{0,div}^{0.31}$ for the closed divertor condition in ASDEX Upgrade. The dependence on other experimental parameters appears relatively weak. The observed trend for increasing $n_{e,sep}$ with plasma current is mainly caused by operational conditions with higher gas puff rates at higher I_p. Under stationary conditions, the divertor pressure can be regarded as engineering parameter being largely proportional to the gas puff rate. The measured relation of $n_{e,sep}$ and $p_{0,div}$ has been approximately reconciled by simple analytical 2-point and 1D considerations. Within a simple 1D model, the upstream separatrix density is determined by the sheath boundary condition at the outer target, the assumption of

Spitzer parallel electron heat conduction and pressure balance. Considering total fluxes rather than flux densities, the 2-point model solution $n_{e,sep} \propto \Gamma_{0,div}^{0.5}$ is modified toward a weaker $p_{0,div}$ dependence by a broadening of the divertor heat flux with increasing neutral pressure. 2D modelling will be required to determine the broadening effects and the physics mechanism which are resonsible for the deviation between simple 1D model and experimental result.

Since extrapolation from the target quite well captures midplane conditions, and also in line with [15], one may cautiously conclude that core fuelling effects are not very important for the value of the separatrix density. Nevertheless, a fueling contribution by the high field side high density is clearly visible, which results in a reduction of $n_{e,sep}$ as well as of the neutral pressure at the HFS divertor region during nitrogen seeding [27]. The fact that the divertor neutral pressure acts as the dominant engineering parameter for the separatrix density, and also determines the outer divertor detachment threshold [10] can serve as a guideline for future optimization of tokamak performance. The separatrix density is limited by H-mode confinement degradation and the H-L transition [8]. With the relation obtained in this work, this limit can also be connected to a divertor neutral pressure limit. The neutral pressure on the other hand is also a leading parameter for the divertor power exhaust and achievement of detachment [9] and can thus be regarded as key engineering parameter in operational scenario optimization. Further work is required on the divertor heat flux broadening (factor b). 2D modelling and possibly additional physics (turbulence, blobs) will have to be considered to understand present experiments and gain a better predictive capability.

7. Acknowledgements

This work has been carried out within the framework of the EUROfusion Consortium and has received funding from the Euratom research and training programme 2014-2018 under grant agreement number 633053. The views and opinions expressed herein do not necessarily reflect those of the European Commission.

8. References

[1] SCHWEINZER, J. et al., Journal of Nuclear Materials **266–269** (1999) 934.
[2] DUNNE, M. G. et al., Plasma Physics and Controlled Fusion **59** (2017) 014017.
[3] LIPSCHULTZ, B. et al., Fusion Science and Technology **51** (2007) 369.
[4] REINKE, M., Nucl. Fusion (2017) 034004.
[5] GOLDSTON, R. et al., Plasma Phys. Controlled Fusion (2017) 055015.
[6] PSHENOV, A. et al., Phys. Plasmas **24** (2017) 072508.
[7] BERNERT, M. et al., Plasma Physics and Controlled Fusion **57** (2015) 014038.
[8] EICH, T. et al., Correlation of the tokamak H-mode density limit with ballooning stability at the separatrix, submitted to Nuclear Fusion (2017).
[9] KALLENBACH, A. et al., Nuclear Fusion **55** (2015) 053026.
[10] KALLENBACH, A. et al., Plasma Physics and Controlled Fusion **58** (2016) 045013.

[11] SAMM, U. et al., Journal of Nuclear Materials **176-177** (1990) 273.
[12] KALLENBACH, A. et al., Journal of Nuclear Materials **415** (2011) S19.
[13] NEUHAUSER, J. et al., Plasma Physics and Controlled Fusion **44** (2002) 855.
[14] STANGEBY, P. C. et al., Nucl. Fusion **55** (2015) 093014.
[15] LEONARD, A. et al., Nucl. Fusion **57** (2017) 086033.
[16] SUN, H. J. et al., Plasma Physics and Controlled Fusion **59** (2017) 105010.
[17] EICH, T. et al., Phys. Rev. Lett. **107** (2011) 215001.
[18] SUN, H. J. et al., Plasma Physics and Controlled Fusion **57** (2015) 125011.
[19] POTZEL, S. et al., Journal of Nuclear Materials **463** (2015) 541.
[20] EICH, T. et al., Nuclear Fusion **53** (2013) 093031.
[21] ROHDE, V. et al., Plasma Physics and Controlled Fusion **51** (2009) 124033 (8pp).
[22] STANGEBY, P., *The Plasma Boundary of Magnetic Fusion Devices*, Institute of Physics Publishing, Bristol and Philadelphia, 2000.
[23] MAKOWSKI, M. et al., Phys. Plasmas **19** (2012) 056122.
[24] BRIDA, D. et al., Nucl. Fusion **57** (2017) 116006.
[25] KALLENBACH, A. et al., Plasma Physics and Controlled Fusion **52** (2010) 055002.
[26] POTZEL, S. et al., Nuclear Fusion **54** (2014) 013001.
[27] REIMOLD, F. et al., The high field side high density region in SOLPS-modelling of nitrogen-seeded H-mode in ASDEX Upgrade, Nuclear Materials and Energy (2017), http://dx.doi.org/10.1016/j.nme.2017.01.010 .
[28] KRASHENINNIKOV, S., Physics Letters A **283** (2001) 368.
[29] CARRALERO, D. et al., Nuclear Fusion **57** (2017) 056044.